Nitrogen-Doped Graphene/ZnSe Nanocomposites: Hydrothermal Synthesis and Their Enhanced Electrochemical and Photocatalytic Activities

Ping Chen, Tian-Yuan Xiao, Hui-Hui Li, Jing-Jing Yang, Zheng Wang, Hong-Bin Yao, and Shu-Hong Yu*

Division of Nanomaterials and Chemistry, Hefei National Laboratory for Physical Sciences at Microscale, Department of Chemistry, National Synchrotron Radiation Laboratory, University of Science and Technology of China, Hefei, Anhui 230026, People's Republic of China.

ABSTRACT

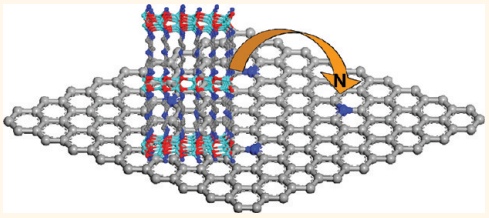

Nitrogen-doped graphene (GN) has great potential applications in many fields because doping with nitrogen can alter the electrical properties of graphene. It is still a challenge to develop a convenient method for synthesis of GN sheets. In this paper, we first report the synthesis of a nitrogen-doped graphene/ZnSe nanocomposite (GN-ZnSe) by a one-pot hydrothermal process at low temperature using graphene oxide nanosheets and $[ZnSe](DETA)_{0.5}$ nanobelts as precursors. ZnSe nanorods composed of ZnSe nanoparticles were found to deposit on the surface of the GN sheets. The results demonstrated that $[ZnSe](DETA)_{0.5}$ nanobelts were used not only as the source of ZnSe nanoparticles but also as the nitrogen source. Interestingly, it was found that the as-prepared nanocomposites exhibit remarkably enhanced electrochemical performance for oxygen reduction reaction and photocatalytic activities for the bleaching of methyl orange dye under visible-light irradiation. This facile and catalyst-free approach for depositing ZnSe nanoparticles onto the graphene sheets may provide an alternative way for preparation of other nanocomposites based on GN sheets under mild conditions, which show their potential applications in wastewater treatment, fuel cells, energy storage, nanodevices, and so on.

KEYWORDS: nitrogen-doped graphene · ZnSe · nanocomposite · photocatalytic activities · oxygen reduction reaction

Since graphene was discovered, it has received great interest because it could be of great use in condensed physics and materials science. As the two-dimensional monolayer form of sp^2-hybridized carbon, graphene has the characteristics of high electron mobility and atomic thickness, so that it promises widespread applications.[1−4] Recently, it has been reported that doping can alter the electrical properties of graphene.[5,6] Li *et al*. reported the synthesis of nitrogen-doped graphene (GN) by using nitrogen plasma treatment of graphene and found that it exhibited high electrocatalytic activity for reduction of hydrogen peroxide and fast direct electron transfer kinetics for glucose oxidase.[7] Kang *et al*. synthesized GN to develop ultracapacitors with excellent cycle life (>200 000), high power capability (close to 280 F/g), and compatibility with flexible substrates.[8] Therefore, GN has great potential applications in many fields. Recently, some methods have been reported to synthesize GN, such as the arc discharge method,[9] chemical vapor deposition (CVD),[10−13] thermal annealing graphene oxide (GO) with NH_3, and graphene treated with nitrogen plasma. In the case of the arc discharge method or nitrogen plasma, rigorous conditions or special instruments are required. CVD is a common method for the synthesis of N-doped graphene. However, the toxicity of the nitrogen precursors (NH_3 and pyridine) and possible contamination of the products by metal catalysts limit the practical application of gas-phase synthesis methods. Therefore, it is still a challenge to prepare GN sheets by a facile method.[8,14]

Semiconductor nanostructures have attracted intensive interest due to their fundamental importance as well as their enormous potential in optoelectronic, magnetic, and catalytic applications.[15,16] Zinc selenide (ZnSe) is a direct band gap semiconductor with a band gap energy of 2.7 eV and is regarded as a good candidate for short-wavelength lasers, blue laser diodes,

* Address correspondence to shyu@ustc.edu.cn.

Received for review October 31, 2011 and accepted December 2, 2011.

Published online December 02, 2011
10.1021/nn204191x

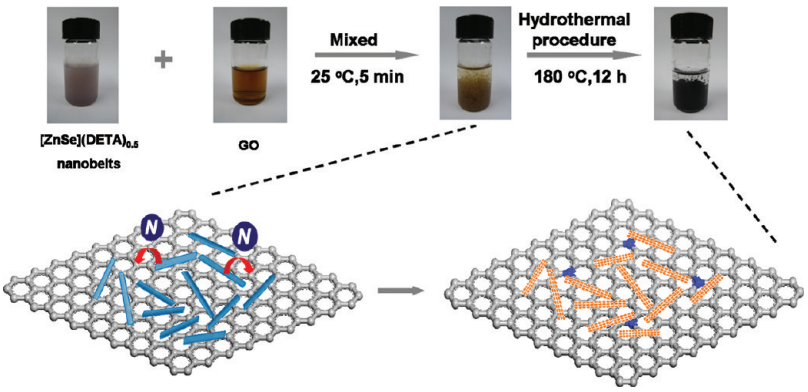

Scheme 1. Schematic illustration of the preparation of GN-ZnSe nanocomposites (blue rods, [ZnSe](DETA)$_{0.5}$ nanobelts; orange rods, ZnSe nanorods; purple balls, N; gray balls, C).

light-emitting diodes, and tunable mid-IR laser sources.[17] Recently, zero-dimensional ZnSe nanoparticles, one-dimensional ZnSe nanowires, and two-dimensional ZnSe thin films have been extensively researched.[18,19] We have prepared uniform and well-defined ZnSe-(diethylenetriamine)$_{0.5}$ ([ZnSe](DETA)$_{0.5}$) nanobelts by hydrazine-hydrate-assisted solvothermal reactions in a ternary solution. The nanobelt is an inorganic−organic hybrid material, which consists of ZnSe slabs sandwiched by coordinated diethylenetriamine layers.[20]

It has been reported that graphene incorporated with nanoparticles, such as Pt, Au, Ag, TiO_2, ZnO, CeO_2, MnO_2, and CdS, shows high activity for catalytic applications in electrochemical catalysis,[21] fuel cells,[11,22] capacitors,[23−25] photocatalytic degradation,[26,27] photovoltaic devices,[28] *etc*. Since graphene nanocomposites can exhibit enhanced performance, it has become a priority for researchers to prepare these nanocomposites.[29,30] However, to our best knowledge, little work has been done on N-doped graphene/semiconductor nanocomposites.

In this article, we report a new strategy to synthesize nitrogen-doped graphene/ZnSe (GN-ZnSe) nanocomposites. ZnSe was deposited on the surface of GN in the shape of nanorods, which were composed of ZnSe nanoparticles. In the synthesis procedure, [ZnSe]-(DETA)$_{0.5}$ nanobelts were used not only as the ZnSe source but also as the nitrogen source. Interestingly, it was found that the electrochemical performance and photocatalytic activities of the as-prepared nanocomposites could be remarkably enhanced. The products have potential applications such as in wastewater treatment, fuel cells, energy storage, and nanodevices.

RESULTS AND DISCUSSION

The preparation procedure of GN-ZnSe nanocomposites (GN-ZnSe) is shown in Scheme 1. [ZnSe](DETA)$_{0.5}$ nanobelts were gradually dropped into the GO solution, and the mixture solution was stirred magnetically at 25 °C for 5 min and transferred into an autoclave with a volume of 50 mL. When the [ZnSe](DETA)$_{0.5}$ nanobelts were gradually dropped into the GO solution, sediments were produced immediately because of the electrostatic interaction between the nanobelts and GO. Then the sediments were processed by a one-pot hydrothermal procedure at 180 °C for 12 h, and the GN-ZnSe nanocomposites were obtained. This is a simple and catalyst-free method to prepare nitrogen-doped graphene/semiconductor nanocomposites.

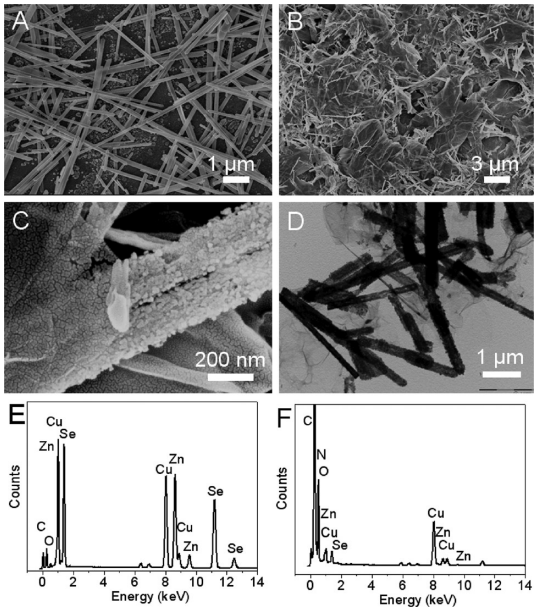

Figure 1. (A) SEM image of the [ZnSe](DETA)$_{0.5}$ nanobelts; (B) SEM image of GN-ZnSe; (C) magnified SEM image of GN-ZnSe; (D) TEM image of GN-ZnSe; (E) EDX spectrum of the ZnSe nanorods in GN-ZnSe; (F) EDX spectrum of the graphene in GN-ZnSe.

Figure 1A show representative SEM images of the [ZnSe](DETA)$_{0.5}$ nanobelts. The nanobelts are about 20−40 nm thick and have lengths ranging up to 10−15 um and uniform diameters of 200−300 nm. The surfaces of the nanobelts are smooth. Figure S1 shows the AFM height images of GO. From Figure S1, the average thickness of the GO is about 1.1 nm. The morphologies of GN-ZnSe are shown in Figure 1B, C,

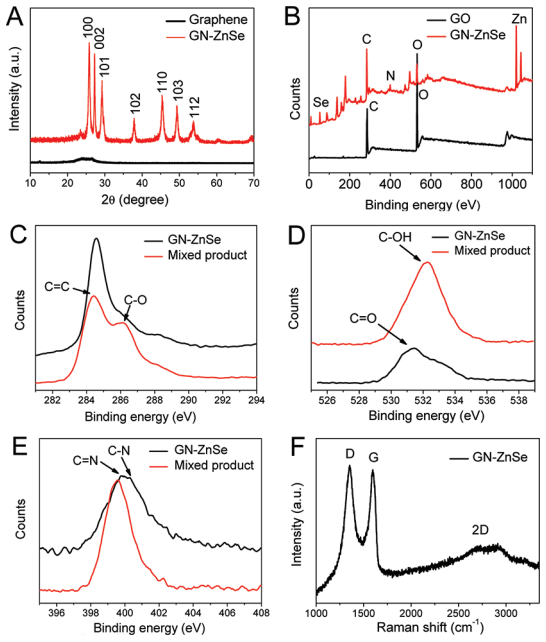

Figure 2. (A) XRD patterns of graphene and the GN-ZnSe composite, respectively; (B) XPS survey spectra of GN-ZnSe and GO; (C) high-resolution XPS spectra of the C1s region for GN-ZnSe and the mixed product; (D) high-resolution XPS spectra of the O1s region for GN-ZnSe and the mixed product; (E) high-resolution XPS spectra of the N1s region for GN-ZnSe and the mixed product; (F) Raman spectrum of the GN-ZnSe nanocomposite.

and D. It is seen that ZnSe was deposited on the surface of graphene in the shape of nanorods. The ZnSe nanorods have lengths ranging up to 1−4 μm and diameters of 150−250 nm. The ZnSe nanorods are composed of ZnSe nanoparticles with a diameter of 10−15 nm. Figure 1E and F shows the energy dispersive X-ray (EDX) images of the ZnSe nanorods and graphene in GN-ZnSe, respectively. These results further confirm the presence of Zn and Se elements on the nanorods and the presence of N element on the graphene. The thickness of the graphene in the nanocomposite was evaluated by AFM, and the average thickness of the graphene in the nanocomposite is about 1.2 nm, corresponding to four layers (see Supporting Information, Figure S2).

The typical XRD pattern of the GN-ZnSe nanocomposite is shown in Figure 2A, which is in good agreement with the JCPDS card (no. 89-2940). The main diffraction peaks can be indexed to hexagonal structure (a = 3.996 Å, c = 6.626 Å), corresponding to a hexagonal ZnSe phase. X-ray photoelectron spectroscopy (XPS) was used to confirm the formation of graphene from GO through a hydrothermal process. Figure 2B shows the full-scale XPS spectra of GN-ZnSe and GO. From the Figure 2B, the XPS spectrum for the GN-ZnSe sample shows O1s at 532.05 eV, Zn2p3 at 1021.0 eV, and Se3d at 54.5 eV. Figure 2C shows the high-resolution XPS spectra of the C1s region for GN-ZnSe and the mixed product of the $[ZnSe](DETA)_{0.5}$ nanobelts and GO solution. One main peak located at 284.7 eV in the high-resolution XPS spectrum of the C1s region for GN-ZnSe was observed, corresponding to sp^2-hybridized graphitic carbon atoms. In the XPS spectrum of the C1s region for the GO, the main peaks are located at 284.5 and 286.3 eV. The peaks at 284.5 and 286.3 eV are attributed to sp^2 carbon and C−O bonding configurations, respectively. Figure 2D shows the high-resolution XPS spectra of the O1s region for GN-ZnSe and the mixed product. The XPS spectrum of the O1s region for GN-ZnSe shows one main peak at 530.9−531.3 eV, corresponding to C═O. In the XPS spectrum of the O1s region for the mixed product, the main peak is at 532.4 eV, which corresponds to C−OH. It is seen that the peak intensity at 532.4 eV decreased after the sample was hydrothermally treated. Figure 2C and D indicates that most oxygen groups of the GO in the mixed product have been removed by the synthesis procedure. The high-resolution XPS spectra of the N1s region for GN-ZnSe and the mixed product are shown in Figure 2E. For the mixed product, the main peak is at 399.5 eV. However, for GN-ZnSe, the main peaks are at 399.9 and 400.2 eV, which are attributed to C═N and C−N bonding configurations, respectively. The peak at 400.2 eV corresponds to pyrrolic-N.[9,10] These results confirm the formation of N-doped graphene from GO. Figure 2B, C, D, and E clearly demonstrates the formation of GN-ZnSe from the mixture of the $[ZnSe](DETA)_{0.5}$ nanobelts and GO solution by a hydrothermal process. The Raman spectrum of the nanocomposite in Figure 2F indicates the existence of the D band located at 1348 cm^{-1} and the G band located at 1595 cm^{-1}. In addition, a broader 2D peak appeared at around 2683 cm^{-1}, which is consistent with that of the few-layer nitrogen-doped graphene reported by Xia *et al.*[31]

So far, some methods have been reported to synthesize nitrogen-doped graphene, such as the arc charge method[9] and chemical vapor deposition.[10−13] However, these methods require rigorous conditions or special instruments. In our proposed strategy, the GN-ZnSe nanocomposite can be prepared easily at a low temperature. As many hybrid semiconductor nanobelts and nanostructures have been synthesized recently,[32−34] the present facile approach may be readily extended to the preparation of other kinds of semiconducting nanocomposites based on graphene sheets.

The influence of the reaction temperature on the morphologies of the products has been investigated. From Figure 3A, B and Figure 1C, it can be concluded that the reaction temperature plays a crucial role in the formation of GN-ZnSe. It is found that when the temperature is below 140 °C, the GN-ZnSe nanocomposite cannot form. When the temperature is 160 °C, some of the $[ZnSe](DETA)_{0.5}$ nanobelts still exist, but when the temperature increases to 200 °C, the ZnSe nanorods composed of ZnSe nanoparticles will collapse.

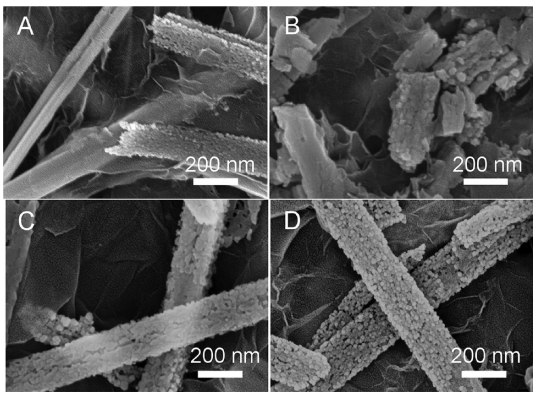

Figure 3. SEM images of the samples prepared under different conditions: (A) 160 °C, 12 h, weight ratio of [ZnSe](DETA)$_{0.5}$ to GO (w/w) of 1:1; (B) 200 °C, 12 h, weight ratio of [ZnSe](DETA)$_{0.5}$ to GO (w/w) of 1:1; (C) 180 °C, 12 h, ratio of [ZnSe](DETA)$_{0.5}$ to GO (w/w) of 1:4; (D) 180 °C, 12 h, ratio of [ZnSe](DETA)$_{0.5}$ to GO (w/w) of 2:1.

In addition, the weight ratio of [ZnSe](DETA)$_{0.5}$ to GO (w/w) also plays an important role. By controlling this ratio, the N percentage in the GN-ZnSe nanocomposites can be tuned. The highest atomic percentage of N (6.7%) can be reached according to the XPS analysis. Figure 3C and D shows the SEM images of the nanocomposites with N percentage of 2.6% and 6.6%, respectively.

The zeta potential of the GO solution (0.5 mg/mL) and the [ZnSe](DETA)$_{0.5}$ hybrid nanobelt solution (0.5 mg/mL) is −24.49 and 11.84 mV, respectively, indicating that the GO sheet in solution is negatively charged, but the [ZnSe](DETA)$_{0.5}$ hybrid nanobelt is positively charged.

According to the above discussion, the preliminary formation mechanism of GN-ZnSe was proposed and is shown in Scheme 1. First, when the [ZnSe](DETA)$_{0.5}$ hybrid nanobelts are gradually dropped into the GO solution, the nanobelts will deposit on the surface of GO because of the electrostatic interactions between the nanobelt and GO, and sediments will form immediately. Then, diethylenetriamine (DETA) can be extracted from [ZnSe](DETA)$_{0.5}$ nanobelts in the hydrothermal procedure. This DETA not only has sufficient reducing capability on the formation of graphene from GO but also plays a role in nitrogen-doping for the formation of GN. This leads to *in situ* formation of ZnSe nanorods on the GN.[35,36] Therefore, the GN-ZnSe nanocomposites can be obtained.

The oxygen reduction reaction (ORR) is very important in fuel cells and other electrochemical devices.[37,38] Recently, some effective and low-cost ORR electrocatalysts have been investigated.[39,40] N-Doped graphene was demonstrated as a promising Pt-free catalyst in electrocatalytic applications of ORR.[11,12] We tested rotating disk electrode (RDE) voltammograms to research the electrocatalytic activities of GN- ZnSe for ORR in O_2-saturated 1.0 M KOH solution at room temperature. Figure 4A displays the ORR curves of the graphene, GN-ZnSe, and the directly mixed product of GO and ZnSe nanobelts. For the pure graphene electrode and directly mixed product of GO and ZnSe nanobelts electrode, the values of the onset potential was −185 and −180 mV, respectively. They exhibit similar onset potentials and reduction currents for ORR. However, the value of onset potential at the GN-ZnSe electrode was about −80 mV. Clearly, the GN-ZnSe electrode exhibits more positive onset potential and much larger current for ORR. The positive shift of the onset potential and enhancement of the reduction current for ORR on the GN-ZnSe electrode indicate that the GN-ZnSe electrode possesses much higher electrocatalytic activity toward ORR than pure graphene. The XPS data of GN-ZnSe show that the N1s peak has one component centered at 400.2 eV corresponding to pyrrolic-N. It has been reported that the presence of pyridine-like and pyrrolic nitrogen atoms within the graphene structure plays a role in the ORR process.[11] We propose that the pyrrolic nitrogen atoms within the GN-ZnSe nanocomposite will play a role in the electrocatalytic activity. Figure 4B shows the RDE voltammograms for the ORR on the GN-ZnSe electrode at various rotation speeds. With an increase of the rotation speed, the reduction current increases. The kinetic parameters can be analyzed with the Koutecky−Levich equations using the following relationship:

$$\frac{1}{i} = \frac{1}{i_k} + \frac{1}{B\omega^{1/2}}$$

where i is the measured current, i_k is the kinetic current, and ω is the electrode rotation rate. The theoretical value of the Levich slope (B) is evaluated from the following relationship:

$$B = 0.62nFC_{O_2}D_{O_2}\nu^{-1/6}$$

where n is the overall number of transferred electrons in the ORR process, F is the Faradaic constant (96500 C/mol), C_{O2} is the oxygen concentration (solubility) in 1 M KOH (0.83×10^{-6} mol cm^{-3}), D_{O2} is the oxygen diffusion coefficient in 1 M KOH (1.34×10^{-5} cm^2 s^{-1}), and ν is the kinematic viscosity of the 1 M KOH (0.01 cm^2 s^{-1}).[41] Figure 4B (inset) shows the corresponding Koutecky−Levich plots (i^{-1} vs $\omega^{-1/2}$) and its good linearity. At the GN-ZnSe electrode, the number of electrons transferred was estimated to be 3.1−3.3 at potentials ranging from −0.3 to −0.6 V. However, according to the literature reported, the number of transferred electrons for the graphene in the ORR process is about 2.2.[12] The electrochemical reduction of O_2 has two main possible pathways: one is the transfer of two electrons to produce H_2O_2, and the other is a direct four-electron pathway to produce water. It is highly desirable to reduce O_2 *via* the 4e-electron pathway to obtain maximum energy capacity.[42] Therefore, different from the graphene electrode, the GN-ZnSe electrode reveals a close four-electron pathway for ORR with much higher peak current. Recently, single-layer graphene

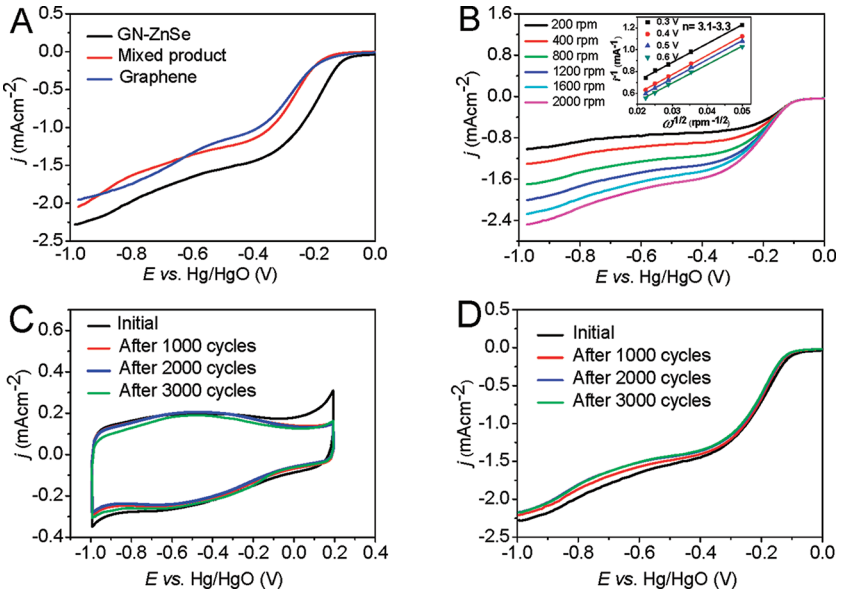

Figure 4. (A) RDE voltammograms for the ORR in O_2-saturated 1.0 M KOH solution at room temperature (rotation speed 1600 rpm, sweep rate 20 mV s^{-1}) at the pure graphene electrode, GN-ZnSe electrode, and directly mixed product of GO and ZnSe nanobelts electrode; (B) RDE voltammograms for the ORR at the GN-ZnSe electrode at various rotation speeds and Koutecky–Levich plots (i^{-1} vs $\omega^{-1/2}$) at different electrode potentials (inset); (C) CVs for the ORR at the GN-ZnSe electrode after 3000 cycles (sweep rate 50 mV s^{-1}); (D) RDE voltammograms for the ORR at the GN-ZnSe electrode after 3000 cycles (rotation speed 1600 rpm, sweep rate 20 mV s^{-1}).

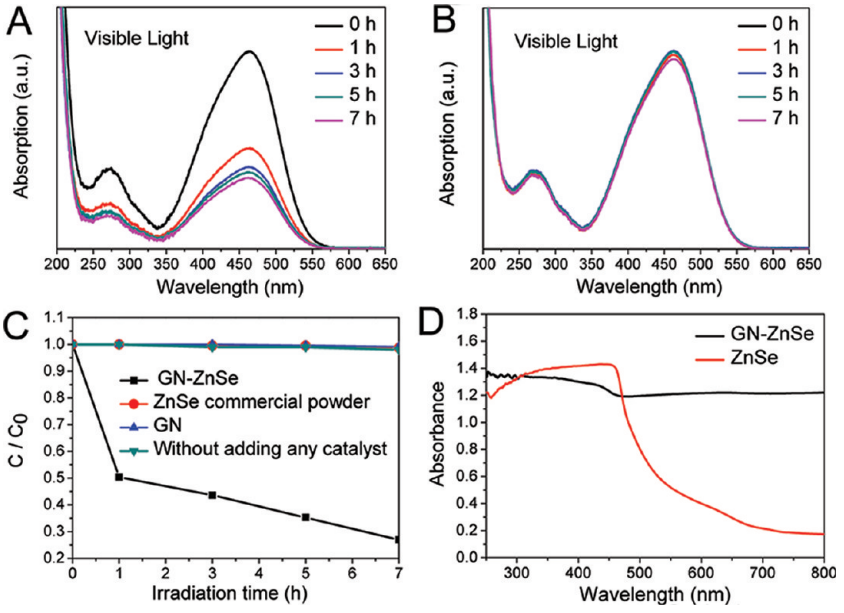

Figure 5. (A) UV–visible absorption spectra for MO solutions under visible light in the presence of GN-ZnSe; (B) UV–visible absorption spectra of the MO solutions under visible light in the presence of commercial ZnSe powder; (C) photobleaching curves of MO in water under visible light in the presence of GN-ZnSe, ZnSe commercial powder, and GN, and without adding any catalyst; (D) diffuse reflectance UV–vis spectra of ZnSe commercial powder and GN-ZnSe. The GN was obtained from GN-ZnSe by the treatment of hydrochloric acid. XPS data show the Zn and Se content in the GN was zero, but the N content was almost same as that in GN-ZnSe.

doped with pure pyridinic N was synthesized by thermal chemical vapor deposition of hydrogen and ethylene on Cu foils in the presence of ammonia, but the two-electron reduction mechanism of ORR on the doped graphene was described.[12] Although there have been reports on the synthesis of nitrogen-doped graphene with a similar four-electron reduction process leading to the formation of H_2O, these synthesis procedures require rigorous conditions or special instruments.[42]

The durability of the electrocatalytic materials has been regarded as one of the most important issues.[43] The electrochemical stability of the GN-ZnSe electrode

toward ORR was also examined. Figure 4C and D shows the CVs and RDE voltammograms for the ORR at the GN-ZnSe electrode after 3000 cycles. It is clear that no obvious decrease in current occurred after 3000 continuous cycles, indicating that the GN-ZnSe catalyst is stable.

For the absorption of a more solar beam and practical applications of the photocatalysts, the exploration of new visible-light-responsive photocatalysts with high photoactivity is currently an intensive and hot research topic.[44,45] Recently, the photocatalytic activities of ZnSe nanostructures have been reported; however, it is still a challenge to develop new ZnSe nanostructures and improve the photocatalytic activities under visible-light irradiation.[19,46] Photocatalytic activities of GN-ZnSe for bleaching of methyl orange (MO) dye under visible-light irradiation ($\lambda > 420$ nm) were tested in a 100 mL beaker that contained the reaction slurry (50 mL). In each experiment, 15 mg of sample was added into 50 mL of MO solution (5×10^{-5} M). Then, the suspension was stirred and exposed to visible-light irradiation for various durations. The characteristic absorption of MO at 463 nm was selected to measure the photocatalytic ability. Figure 5A, B and Figure S3 show the UV−visible absorption spectral changes observed for the MO solutions in the presence of GN-ZnSe, ZnSe commercial powder, and GN, respectively. After treatment for 7 h by the GN-ZnSe nanocomposite, the bleaching of MO reaches 71.50%. However, almost no bleaching of MO was found if treated by commercial ZnSe powder. Figure 5C shows the photobleaching curves of MO in water under visible light in the presence of GN-ZnSe, commercial ZnSe powder, and GN, and without adding any catalyst. These data suggest that GN-ZnSe has remarkable photocatalytic activity for the bleaching of MO dye under visible-light irradiation, while commercial ZnSe powder and GN do not have obvious photocatalytic activity, respectively.

Three factors are crucial for the photocatalytic activities of the composite. They are the adsorption of contaminant molecules, light irradiation absorption, and charge transportation and separation.[27] We measured the adsorption of MO molecules by GN-ZnSe and commercial ZnSe powder, respectively. After treating for 8 h, nearly 30.72% of the initial dye was absorbed on the GN-ZnSe composite (15 mg), while only 7.84% of the initial dye was absorbed by commercial ZnSe powder (15 mg). That is to say, GN-ZnSe showed a better adsorption ability than commercial ZnSe powder. The absorption range of light has an important role in the visible-light photobleaching of contaminant molecules. Some reports show that a more efficient utilization of the solar spectra can be obtained by extending the photoresponding range. Figure 5D shows the diffuse reflectance UV−vis spectra of commercial ZnSe powder and the GN-ZnSe composite. From Figure 5D, an obviously extended photoresponding range was achieved for GN-ZnSe. Recently, it has been reported that nitrogen-doping can open the band gap of graphene and convert graphene into a semiconductor.[5,14] Therefore, the present GN-ZnSe system is a heterosystem with two semiconductors (GN/ZnSe) that create p−n junctions. This system promotes charge collection and separation at the interfaces and thus improves the bleaching of contaminant molecules.

From the above discussion, we believe that there are three reasons for the remarkable photocatalytic activity of GN-ZnSe for the bleaching of MO dye under visible-light irradiation. First, GN-ZnSe has enhanced adsorption MO molecules; second, GN-ZnSe has an obviously extended photoresponse range; finally, the GN/ZnSe heterosystem is formed. Because the GN-ZnSe system has remarkable photocatalytic activity for the bleaching of MO dye under visible-light irradiation and excellent absorption ability for MO molecules from the solution, it may have practical applications in the removal of contaminants.

CONCLUSION

In summary, a kind of GN-ZnSe nanocomposite can be synthesized by a facile, catalyst-free approach at a low temperature, in which $[ZnSe](DETA)_{0.5}$ nanobelts were used not only as the ZnSe nanoparticle source but also as the nitrogen source. ZnSe was deposited on the surface of the graphene in a shape of nanorods, each of which was composed of ZnSe nanoparticles. It was found that the electrochemical performance for ORR of the nanocomposites can be enhanced, and the nanocomposites also show remarkable photocatalytic activities for the bleaching of MO. Because many hybrid semiconductor nanobelts and nanostructures have recently been synthesized, the present approach could be readily extended to the preparation of other new nanocomposites based on graphene sheets, which may allow it to have possible applications such as in wastewater treatment, fuel cells, and nanodevices.

METHODS

All reagents are of analytical grade and used without further purification.

Synthesis of GO. GO was prepared by oxidation of graphite under acidic conditions according to the Hummers method.[47]

Synthesis of $[ZnSe](DETA)_{0.5}$ Nanobelts. $[ZnSe](DETA)_{0.5}$ nanobelts were synthesized according to a method reported previously.[20] Briefly, $ZnSO_4 \cdot 7H_2O$ (0.05 mmol) and Na_2SeO_3 (0.05 mmol) were added into a mixed solution (35 mL) with a volume ratio of $V_{N2H4 \cdot H2O}/V_{DETA}/V_{H2O}$ = 5:14:16 under stirring. The mixed solution was transferred into a Teflon-lined autoclave with a volume of 50 mL. Hydrothermal treatment of the mixed solution was done at 180 °C for 12 h, and then white floccules formed after the reaction was washed with distilled

water and absolute ethanol and dried under vacuum at 80 °C for 6 h.

Synthesis of GN-ZnSe Nanocomposite. In a typical process, 17 mg of $[ZnSe](DETA)_{0.5}$ nanobelts was dispersed with 17 mL of distilled water, and 18 mg of graphene oxide was dispersed with 18 mL of distilled water. Then, the $[ZnSe](DETA)_{0.5}$ nanobelt solution was gradually added to the GO solution. The solution mixture was stirred magnetically at 25 °C for 5 min and transferred into an autoclave with a volume of 50 mL. Hydrothermal treatment of the mixed solution was done at 180 °C for 12 h, and the solid product was separated by centrifugation and washed with distilled water and ethanol several times. Then, the GN-ZnSe nanocomposites were obtained.

Characterization. Scanning electron microscopy (SEM) was carried out with a field emission scanning electron microanalyzer (JEOL-6700F). Transmission electron microscopy (TEM) images were recorded on a JEOL-F2010 with an EDX analytical system. UV−vis spectra were recorded on an UV-2501PC/2550 spectrophotometer at room temperature (Shimadzu Corporation, Japan). Diffuse reflectance UV−vis spectra were measured on a DUV-SOLID3700 spectrophotometer (Shimadzu Corporation, Japan). X-ray photoelectron spectroscopic measurements were performed on an X-ray photoelectron spectrometer (ESCALab MKII). X-ray diffraction (XRD) of the products was performed on a Philips X'Pert PRO SUPER X-ray diffractometer with Cu radiation (1.406 Å). Zeta-potential values were recorded using a Zeta Sizer 3000 HS (Malvern Instruments). Raman spectra were taken by a Renishaw System 2000 spectrometer with a 514.5 nm laser excitation. An atomic force microscope (Nanoscope IIIa; Digital Instruments) was used to measure the morphology of the sample. A Si_3N_4 tip was used in the contact mode (Nanoprobes, Digital Instruments Inc.).

ORR Activities. The electrochemical measurements were carried out in a conventional three-electrode cell using an IM6e electrochemical workstation (Zahner-Electrik, Germany) controlled at room temperature. A glassy carbon (GC) disk with a diameter of 5 mm served as the substrate for the working electrode, with the rotating rate varying from 200 to 2000 rpm. Hg/HgO and platinum wire were used as reference and counter electrodes, respectively. An 8.3 mg amount of the sample was dispersed in an ethanol solution (10 mL) ultrasonically for 15 min. A 15 μL amount of this suspension was dropped and adhered on the GC disk electrode using Nafion solution (5 μL, 0.05 wt %). The oxygen reduction tests were carried out in O_2-saturated 1.0 M KOH solution at room temperature.

Photocatalytic Activities. Photocatalytic activities of GN-ZnSe for bleaching of MO under visible-light irradiation were tested. For each experiment, 15 mg of sample was added into a beaker containing 50 mL of 5×10^{-5} M MO solution. A 500 W Xe lamp equipped with a 420 nm cut-off filter was used as a light source to provide visible-light irradiation ($\lambda > 420$ nm). Before the visible-light irradiation, the solutions were continuously stirred for about 10 h at room temperature to ensure the establishment of an equilibrium among the MO, water, and the photocatalyst. The distance from the Xe lamp to the reaction slurry was fixed as about 6 cm. Then the suspension was stirred and exposed to visible-light irradiation, and the temperature was kept at room temperature. A MO solution in the reaction slurries was obtained by a microperforated filter, and the concentration of the MO was measured by using a UV−vis spectrophotometer.

Acknowledgment. S.H.Y acknowledges the funding support from the National Basic Research Program of China (2010-CB934700), the National Natural Science Foundation of China (Nos. 91022032, 50732006), International Science & Technology Cooperation Program of China (2010DFA41170), and the Principle Investigator Award by the National Synchrotron Radiation Laboratory at the University of Science and Technology of China. P.C. acknowledge the National Science Foundation for Postdoctoral Scientists (No. 1470).

Supporting Information Available: This material is available free of charge via the Internet at http://pubs.acs.org.

REFERENCES AND NOTES

1. Novoselov, K. S.; Geim, A. K.; Morozov, S. V.; Jiang, D.; Zhang, Y.; Dubonos, S. V.; Grigorieva, I. V.; Firsov, A. A. Electric Field Effect in Atomically Thin Carbon Films. *Science* **2004**, *306*, 666–669.
2. Novoselov, K. S.; Geim, A. K.; Morozov, S. V.; Jiang, D.; Katsnelson, M. I.; Grigorieva, I. V.; Dubonos, S. V.; Firsov, A. A. Two-Dimensional Gas of Massless Dirac Fermions in Graphene. *Nature* **2005**, *438*, 197–200.
3. Geim, A. K. Graphene: Status and Prospects. *Science* **2009**, *324*, 1530–1534.
4. Zhu, Y. W.; Murali, S.; Stoller, M. D.; Ganesh, K. J.; Cai, W. W.; Ferreira, P. J.; Pirkle, A.; Wallace, R. M.; Cychosz, K. A.; Thommes, M.; *et al*. Carbon-Based Supercapacitors Produced by Activation of Graphene. *Science* **2011**, *332*, 1537–1541.
5. Wang, X. R.; Li, X. L.; Zhang, L.; Yoon, Y.; Weber, P. K.; Wang, H. L.; Guo, J.; Dai, H. J. N-Doping of Graphene through Electrothermal Reactions with Ammonia. *Science* **2009**, *324*, 768–771.
6. Ci, L.; Song, L.; Jin, C. H.; Jariwala, D.; Wu, D. X.; Li, Y. J.; Srivastava, A.; Wang, Z. F.; Storr, K.; Balicas, L.; *et al*. Atomic Layers of Hybridized Boron Nitride and Graphene Domains. *Nat. Mater.* **2010**, *9*, 430–435.
7. Wang, Y.; Shao, Y. Y.; Matson, D. W.; Li, J. H.; Lin, Y. H. Nitrogen-Doped Graphene and Its Application in Electrochemical Biosensing. *ACS Nano* **2010**, *4*, 1790–1798.
8. Jeong, H. M.; Lee, J. W.; Shin, W. H.; Choi, Y. J.; Shin, H. J.; Kang, J. K.; Choi, J. W. Nitrogen-Doped Graphene for High-Performance Ultracapacitors and the Importance of Nitrogen-Doped Sites at Basal Planes. *Nano Lett.* **2011**, *11*, 2472–2477.
9. Panchokarla, L. S.; Subrahmanyam, K. S.; Saha, S. K.; Govindaraj, A.; Krishnamurthy, H. R.; Waghmare, U. V.; Rao, C. N. R. Synthesis, Structure, and Properties of Boron- and Nitrogen-Doped Graphene. *Adv. Mater.* **2009**, *21*, 4726–4730.
10. Wei, D. C.; Liu, Y. Q.; Wang, Y.; Zhang, H. L.; Huang, L. P.; Yu, G. Synthesis of N-Doped Graphene by Chemical Vapor Deposition and Its Electrical Properties. *Nano Lett.* **2009**, *9*, 1752–1758.
11. Qu, L. T.; Liu, Y.; Baek, J. B.; Dai, L. M. Nitrogen-Doped Graphene as Efficient Metal-Free Electrocatalyst for Oxygen Reduction in Fuel Cells. *ACS Nano* **2010**, *4*, 1321–1326.
12. Luo, Z. Q.; Lim, S. H.; Tian, Z. Q.; Shang, J. Z.; Lai, L. F.; MacDonald, B.; Fu, C.; Shen, Z. X.; Yu, T.; Lin, J. Y. Pyridinic N Doped Graphene: Synthesis, Electronic Structure, and Electrocatalytic Property. *J. Mater. Chem.* **2011**, *21*, 8038–8044.
13. Imamura, G.; Saiki, K. Synthesis of Nitrogen-Doped Graphene on Pt(111) by Chemical Vapor Deposition. *J. Phys. Chem. C* **2011**, *115*, 10000–10005.
14. Li, X. L.; Wang, H. L.; Robinson, J. T.; Sanchez, H.; Diankov, G.; Dai, H. J. Simultaneous Nitrogen Doping and Reduction of Graphene Oxide. *J. Am. Chem. Soc.* **2009**, *131*, 15939–15944.
15. Alivisatos, A. P. Semiconductor Clusters, Nanocrystals, and Quantum Dots. *Science* **1996**, *271*, 933–937.
16. Nirmal, M.; Brus, L. Luminescence Photophysics in Semiconductor Nanocrystals. *Acc. Chem. Res.* **1999**, *32*, 407–414.
17. Hines, M. A.; Guyot-Sionnest, P. Bright UV-Blue Luminescent Colloidal ZnSe Nanocrystals. *J. Phys. Chem. B* **1998**, *102*, 3655–3657.
18. Peng, Q.; Dong, Y. J.; Li, Y. D. ZnSe Semiconductor Hollow Microspheres. *Angew. Chem., Int. Ed.* **2003**, *42*, 3027–3030.
19. Zhang, L. H.; Yang, H. Q.; Yu, J.; Shao, F. H.; Li, L.; Zhang, F. H.; Zhao, H. Controlled Synthesis and Photocatalytic Activity of ZnSe Nanostructured Assemblies with Different Morphologies and Crystalline Phases. *J. Phys. Chem. C* **2009**, *113*, 5434–5443.
20. Yao, W. T.; Yu, S. H.; Huang, X. Y.; Jiang, J.; Zhao, L. Q.; Pan, L.; Li, J. Nanocrystals of an Inorganic-Organic Hybrid Semiconductor: Formation of Uniform Nanobelts of $[ZnSe](Diethylenetriamine)_{0.5}$ in a Ternary Solution. *Adv. Mater.* **2005**, *17*, 2799–2802.

21. Zheng, J. B.; He, Y. P.; Sheng, Q. L.; Zhang, H. F. DNA as a Linker for Biocatalytic Deposition of Au Nanoparticles on Graphene and Its Application in Glucose Detection. *J. Mater. Chem.* **2011**, *21*, 12873–12879.
22. Xin, Y. C.; Liu, J. G.; Zhou, Y.; Liu, W. M.; Gao, J. A.; Xie, Y.; Yin, Y.; Zou, Z. G. Preparation and Characterization of Pt Supported on Graphene with Enhanced Electrocatalytic Activity in Fuel Cell. *J. Power Sources* **2011**, *196*, 1012–1018.
23. Chen, S.; Zhu, J. W.; Wu, X. D.; Han, Q. F.; Wang, X. Graphene Oxide-MnO(2) Nanocomposites for Supercapacitors. *ACS Nano* **2010**, *4*, 2822–2830.
24. Wang, H. L.; Casalongue, H. S.; Liang, Y. Y.; Dai, H. J. Ni(OH)(2) Nanoplates Grown on Graphene as Advanced Electrochemical Pseudocapacitor Materials. *J. Am. Chem. Soc.* **2010**, *132*, 7472–7477.
25. Wang, Y.; Guo, C. X.; Liu, J. H.; Chen, T.; Yang, H. B.; Li, C. M. CeO(2) Nanoparticles/Graphene Nanocomposite-Based High Performance Supercapacitor. *Dalton Trans.* **2011**, *40*, 6388–6391.
26. Li, B. J.; Cao, H. Q. ZnO@Graphene Composite with Enhanced Performance for the Removal of Dye from Water. *J. Mater. Chem.* **2011**, *21*, 3346–3349.
27. Zhang, H.; Lv, X. J.; Li, Y. M.; Wang, Y.; Li, J. H. P25-Graphene Composite as a High Performance Photocatalyst. *ACS Nano* **2010**, *4*, 380–386.
28. Wang, P.; Jiang, T. F.; Zhu, C. Z.; Zhai, Y. M.; Wang, D. J.; Dong, S. J. One-Step, Solvothermal Synthesis of Graphene-CdS and Graphene-ZnS Quantum Dot Nanocomposites and Their Interesting Photovoltaic Properties. *Nano. Res.* **2010**, *3*, 794–799.
29. Liang, Y. Y.; Li, Y. G.; Wang, H. G.; Zhou, J. G.; Wang, J. J.; Regier, T.; Dai, H. J. Co_3O_4 Nanocrystals on Graphene as a Synergistic Catalyst for Oxygen Reduction Reaction. *Nat. Mater.* **2011**, *10*, 780–786.
30. Zhu, X. J.; Zhu, Y. W.; Murali, S.; Stollers, M. D.; Ruoff, R. S. Nanostructured Reduced Graphene Oxide/Fe(2)O(3) Composite as a High-Performance Anode Material for Lithium Ion Batteries. *ACS Nano* **2011**, *5*, 3333–3338.
31. Sheng, Z. H.; Shao, L.; Chen, J. J.; Bao, W. J.; Wang, F. B.; Xia, X. H. Catalyst-Free Synthesis of Nitrogen-Doped Graphene *via* Thermal Annealing Graphite Oxide with Melamine and Its Excellent Electrocatalysis. *ACS Nano* **2011**, *5*, 4350–4358.
32. Yu, S. H.; Yoshimura, M. Shape and Phase Control of ZnS Nanocrystals: Template Fabrication of Wurtzite ZnS Single-Crystal Nanosheets and ZnO Flake-Like Dendrites from a Lamellar Molecular Precursor ZnS-$(NH_2CH_2CH_2NH_2)$(0.5). *Adv. Mater.* **2002**, *14*, 296–300.
33. Huang, X. Y.; Li, J.; Zhang, Y.; Mascarenhas, A. From 1d Chain to 3d Network: Tuning Hybrid II-VI Nanostructures and Their Optical Properties. *J. Am. Chem. Soc.* **2003**, *125*, 7049–7055.
34. Yao, H. B.; Gao, M. R.; Yu, S. H. Small Organic Molecule Templating Synthesis of Organic-Inorganic Hybrid Materials: Their Nanostructures and Properties. *Nanoscale* **2010**, *2*, 323–334.
35. Zhang, M.; Shi, C.; Zhang, T. K.; Feng, M.; Chang, L.; Yao, W. T.; Yu, S. H. Mn-Substituted [Zn(1-X)Mn(X)Se](DETA)-(0.5) (X=0−0.3) Inorganic-Organic Hybrid Nanobelts: Synthesis, Electron Paramagnetic Resonance Spectroscopy, and Their Temperature- and Pressure-Dependent Optical Properties. *Chem. Mater.* **2009**, *21*, 5485–5490.
36. Yao, H. B.; Li, X. B.; Yu, S. H. New Blue-Light-Emitting Ultralong [Cd(L)(TeO(3))] (L = Polyamine) Organic-Inorganic Hybrid Nanofibre Bundles: Their Thermal Stability and Acidic Sensitivity. *Chem.—Eur. J.* **2009**, *15*, 7611–7618.
37. Lim, B.; Jiang, M. J.; Camargo, P. H. C.; Cho, E. C.; Tao, J.; Lu, X. M.; Zhu, Y. M.; Xia, Y. N. Pd-Pt Bimetallic Nanodendrites with High Activity for Oxygen Reduction. *Science* **2009**, *324*, 1302–1305.
38. Gao, M. R.; Gao, Q.; Jiang, J.; Cui, C. H.; Yao, W. T.; Yu, S. H. A Methanol-Tolerant Pt/CoSe(2) Nanobelt Cathode Catalyst for Direct Methanol Fuel Cells. *Angew. Chem., Int. Ed.* **2011**, *50*, 4905–4908.
39. Gong, K. P.; Du, F.; Xia, Z. H.; Durstock, M.; Dai, L. M. Nitrogen-Doped Carbon Nanotube Arrays with High Electrocatalytic Activity for Oxygen Reduction. *Science* **2009**, *323*, 760–764.
40. Wu, G.; More, K. L.; Johnston, C. M.; Zelenay, P. High-Performance Electrocatalysts for Oxygen Reduction Derived from Polyaniline, Iron, and Cobalt. *Science* **2011**, *332*, 443–447.
41. Tham, M. K.; Walker, R. D.; Gubbins, K. E. Diffusion of Oxygen and Hydrogen in Aqueous Potassium Hydroide Solutions. *J. Phys. Chem.* **1970**, *74*, 1747–1751.
42. Geng, D. S.; Chen, Y.; Chen, Y. G.; Li, Y. L.; Li, R. Y.; Sun, X. L.; Ye, S. Y.; Knights, S. High Oxygen-Reduction Activity and Durability of Nitrogen-Doped Graphene. *Energy Environ. Sci.* **2011**, *4*, 760–764.
43. Zhang, J.; Sasaki, K.; Sutter, E.; Adzic, R. R. Stabilization of Platinum Oxygen-Reduction Electrocatalysts Using Gold Clusters. *Science* **2007**, *315*, 220–222.
44. Asahi, R.; Morikawa, T.; Ohwaki, T.; Aoki, K.; Taga, Y. Visible-Light Photocatalysis in Nitrogen-Doped Titanium Oxides. *Science* **2001**, *293*, 269–271.
45. Chen, X. B.; Liu, L.; Yu, P. Y.; Mao, S. S. Increasing Solar Absorption for Photocatalysis with Black Hydrogenated Titanium Dioxide Nanocrystals. *Science* **2011**, *331*, 746–750.
46. Cao, H. Q.; Xiao, Y. J.; Zhang, S. C. The Synthesis and Photocatalytic Activity of ZnSe Microspheres. *Nanotechnology* **2011**, *22*, 015604.
47. Hummers, W. S.; Offeman, R. E. Preparation of Graphitic Oxide. *J. Am. Chem. Soc.* **1958**, *80*, 1339–1339.